Winter 1-6-2016

Case Study of Quantifying Energy Loss through Ceiling-Attic Recessed Lighting Fixtures through 3D Numerical Simulation

Ri Na
University of Nebraska - Lincoln, rna2@unl.edu

Shengmao Lin
University of Nebraska-Lincoln, linshengmao@gmail.com

Zhigang Shen
University of Nebraska - Lincoln, shen@unl.edu

Linxia Gu
University of Nebraska - Lincoln, gul@fit.edu

A Case Study of Quantifying Energy Loss through Ceiling-Attic Recessed Lighting Fixtures through 3D Numerical Simulation

Ri Na[1], Shengmao Lin[2], Zhigang Shen[1], Ph.D. and Lingxia Gu[2], Ph.D.

[1] The Durham School of Architecture Engineering and Construction, University of Nebraska-Lincoln, Lincoln NE 68588, USA. Email: shen@unl.edu

[2] Department of Mechanical and Materials Engineering, University of Nebraska-Lincoln, Lincoln, NE 68588, USA

Abstract: Air leakage through improperly installed recessed lighting fixtures has been identified as a common issue causing extra energy consumption of residential buildings. However, little quantitative study was found in this area. In this paper, a preliminary evaluation of the magnitude of such energy loss was conducted by numerical simulations using 3D transient CFD model. A typical layout of recessed lighting fixtures was used in this case study with boundary conditions in four different seasons, which were obtained from past measured roof/attic temperature data sets. The results of the numerical simulations indicate that leakage of recessed lighting fixtures could be a very significant channel of energy loss in attic related residential buildings, especially in summer and winter time.

Keywords: energy loss; air leakage; recessed lighting fixtures; attic, CFD

Introduction

Unintended air leakage through buildings' envelopes is one of the common issues negatively affecting the energy performance of residential buildings in the U.S. Air leakage through improperly installed/designed recessed lighting fixtures (RLF) is one of such leakage channels. With understanding the issue Washington State firstly revised its building codes and required all recessed lighting to be strictly air tight (Washington State Building Code Council 2009). The code demanded that air leakage rate of RLF should not exceed 2 CFM (Cubic feet per minute) at 75 Pascals pressure difference, which provided the manufacturers with needed references. Later on, International Energy Conservation Code (IECC) and California also enacted a series of corresponding provisions to regulate the industry standards (International code council 2012; California Energy Commission 2013). Although retrofit projects are not required to comply with all the new provisions, implementing these requirements in existing homes is recommended.

Through physical tests, such as the blower door test and infrared camera techniques, the leaking areas can be detected. However, it is difficult to estimate the quantities of the energy loss through RLF, especially for RLFs mounted underneath the ventilated attics, due to the lack of understanding how airflow works under such conditions. As a result, little quantitative studies were found on even ball-park estimate of energy loss through the improperly installed or designed RLF.

The goal of this research is to provide a quantitative evaluation of the impact of air leakage through RLFs on the energy performance of residential buildings through a case study. For simplicity, the case study only considers the situations in which the light bulbs are not on. But as the authors understand that due to chimney effect when light bulbs are on air flow mass will increase significantly, which is considered as a worse case scenario. The light-bulb-on cases can be to be studied in the further research.

In this paper 3D numerical models were used to simulate the air leakage under different weather conditions, and to provide a rough estimate of the energy loss caused by air leakage through non-IC (Insulation Contact) rated RLFs in terms of magnitude in four different seasons in the Mixed-Humid zone in the U.S. The selection of studying non-IC rated RLFs is due to its large amount in US housing inventory, especially in older houses. The temperature boundary conditions of attics used in this study were provided by USDA's Forest Products Lab (Winandy et. al 2000).

Related Studies

The airtightness is often a stringent requirement for building construction. In an investigation of the air leakage problem in existing buildings, Persily (2004) evaluated a set of 209 dwellings that represent 80% of U.S housing stock to generate frequency distributions of residential infiltration rates. The result of the study indicates that in the U.S residential buildings have become more air tight since 1940. Similarly, Chan et al. (2003) found that the older and smaller houses commonly have higher normalized leakage areas compared to newer and larger ones. The impact of air leakage on heating and cooling loads is significant (Younes, et al, 2011; Jokisalo, J. et. al 2008), especially during winter and summer, when building envelope leakage of residential building could lead to a increases as much as 30-40% of the heating loads and 10-15% of the cooling loads (Emmerich, S. J. 2005).

One common air leakage area is from indoor space to attic space though the canister vents of RLFs, even when the lighting trim is properly sealed (Baker, J., and Lugano, F. 1999; Plympton, P. C et. al 2007; Savers, E. 2006; Van der Meer, 2002). Some serious leakage could even cause ice dam issue. (Armando, L and. McCarthy, S., 2000). In most studies, the potential air leakage areas of the building were usually detected using an infrared thermographic technique during the blower door test (Sherman and Dickerhoff 1998; Balaras and Argiriou 2002). However, very limited quantitative studies was found on evaluating the impact of air leakage from RLF on buildings' energy performance. Numerical methods such as Computational Fluid Dynamics (CFD) became practical in simulating the airflow behavior in both residential and commercial applications (Younes et al., 2012) due to the significant improvement of computation technology from both hardware and software. Compared to experimental study, CFD methods exhibited many advantages in solving air distribution and ventilation related problems in the attic l (Wang, S.et al. 2012; Wang, S. and Shen, Z. 2012 [a, b]).

Methodology

Numerical model

A 3D transient CFD model using commercial software ANSYS Fluent 13.0 was built with boundary conditions from four different seasons. Although the 3D attic geometry model is hypothetical, the weather and temperature boundary conditions are from the actual recorded data by Mississippi Forest Products Laboratory in Starkville, Mississippi in 1999. With these boundary conditions, energy exchange within this attic due to these RLFs was simulated in this case study.

Owing to the buoyancy stableness of the attic ventilation, as well as the symmetrical nature in both geometry and boundary conditions, only a quarter of attic with 9 RLFs is assumed as the computational domain to reduce computational time. The schematic of heat transfer mechanisms in ventilation attic is shown in Fig. 1. Both the convection and radiation are considered in the simulation. To simplify the simulation, the computational domain is only occupied by air, which is assumed to be a Boussinesq fluid with a reference temperature T_o (specified as the outdoor ambient air temperature to adjust the buoyancy effects in the simulation). The pressures at the soffit inlets and ridge vent outlet are specified to be zero gauge (no wind effect). Therefore, the obtained air flow is purely driven by the thermally induced buoyancy forces, i.e., the stack effect. At the soffit inlet, the air is assumed to be ambient air and a turbulent intensity level of 1% (Wang et al. 2012; Wang and Shen 2012 [a,b]).

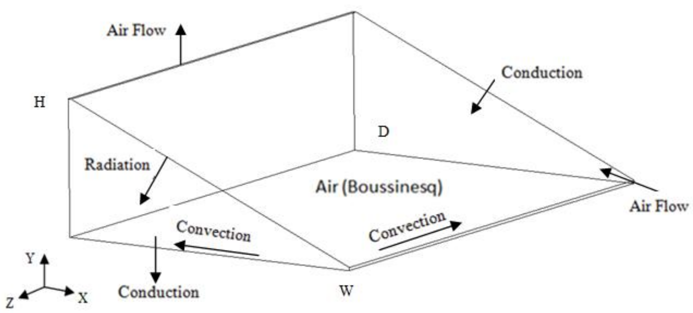

Fig. 1. Schematic of the heat transfer mechanisms in the ventilated attic

The detailed schematic diagram of the RLFs is shown in Fig. 2. The length, width, and height of the attic simulated in the model are 6 m, 4 m, 1.677 m respectively, corresponding to a roof pitch value of 5/12. There are 9 RLFs in the simulated model, which is in accordance with the RFL installation guide from Home Depot (Home Depot 2015). All the recessed light cans are assumed to be non-IC rated to meet the goal of this investigation. The dimensions of the cans were obtained from an actual non-IC rated product bought from Home Depot. The can have four 0.5 cm x 2 cm openings of air leak surround the recessed lighting can (Fig. 3) for heat dissipation generated by the lighting bulb when it is on. The diameter of each lighting can is 15 cm. As a result, the ratio of canister areas V.S. total ceiling area is 0.68: 100. The roof and vertical wall are assumed to be made of 3cm thick ply wood while the ceiling is assumed to be 0.27 cm thick gypsum board covered with15 cm thick fiber insulation.

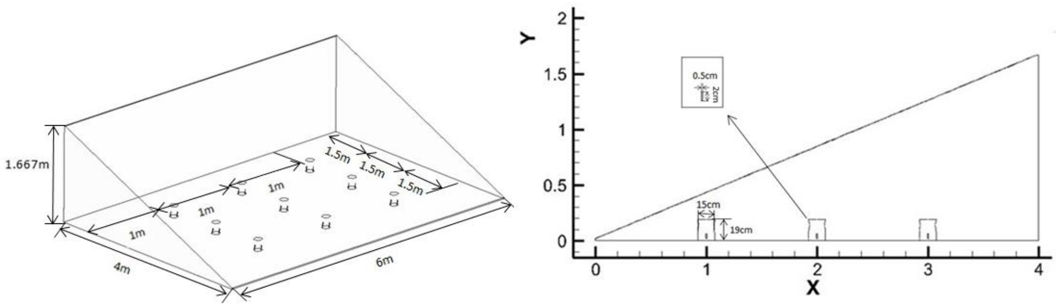

Fig. 2. Geometry of an attic with recessed lighting

Fig. 3. The sample recessed lighting can

Natural ventilation through the attic is assumed in this case. Ventilation ratio refers to the net free area, such as soffit and ridge vent regions, divided by the deck area of the attic (Wang et al., 2012). In this case, the ventilation ratio is set to be 1/200. The insulation level represented by R-value as well as emissivity is also considered in this model as shown in Table 2. All the bounding surfaces in the attics are subjected to the conduction heat transfer. Besides, convection-type boundary conditions are applied to ceiling, roof and vertical wall. In addition, surface-to-surface type radiation boundary conditions are applied to both roof and vertical wall.

Table 2. Boundary conditions

	Thermal Conductivity	**Emissivity**
Roof	R-1.2 (4.733W/m^{2}K)	0.85
Vertical Wall	R-1.2 (4.733W/m^{2}K)	0.85
Ceiling	R-20 (0.284W/m^{2}K)	/

In the attic space, every surface exchanges heat with every other surface through radiation. The energy reflected from surface k is

$$q_{out,k} = \varepsilon_k \sigma \mathrm{T}_\kappa^4 + (1-\varepsilon_k) q_{in,k} \quad (1)$$

where $q_{out,k}$ is the energy flux leaving the surface; ε_k is the emissivity; σ is Boltzmann's constant; $q_{in,k}$ is the energy flux incident on the surface from the surroundings.

The amount of incident energy upon a surface from another surface is the direct function of the surface-to-surface view factor. The view factor F_{ij} between two finite surfaces i and j is given by:

$$F_{ij} = \frac{1}{A_i} \int_{A_i} \int_{A_j} \frac{\cos\theta_i \cos\theta_j}{\pi r^2} \delta_{ij} dA_i dA_j \quad (2)$$

where δ_{ij} is determined by the visibility of dA_j to dA_i. $\delta_{ij}=1$ if dA_j is visible to dA_i and 0 otherwise.

From the view factor reciprocity relationship, the energy flux incident on the surface from the surroundings can be expressed as

$$q_{in,k} = \sum_{j=1}^{N} F_{kj} q_{out,j} \quad (3)$$

Therefore,

$$q_{out,k} = \varepsilon_k \sigma \mathrm{T}_{\kappa}^4 + (1-\varepsilon_k) \sum_{j=1}^{N} F_{kj} q_{out,j} \quad (4)$$

The air flow dynamics was govenred by the momentum and mass conservation equations as below.

Mass: $$\rho_f \Delta \cdot \boldsymbol{v} = 0 \quad (5)$$

Momentum: $$\rho_f \frac{\partial \boldsymbol{v}}{\partial t} + \rho_f ((\boldsymbol{v} - \dot{\boldsymbol{d}}_f) \cdot \nabla) \boldsymbol{v} = \nabla \cdot \boldsymbol{\tau}_f + \boldsymbol{f}_f^B \quad (6)$$

where ρ_f is the fluid density, $\boldsymbol{\tau}_f$ is the fluid stress tensor, $\boldsymbol{f}_f^B$ are the body forces per unit volume, $\boldsymbol{v}$ is the fluid velocity vector, $\dot{\boldsymbol{d}}_f$ is the moving coordinate velocity and $\boldsymbol{v}-\dot{\boldsymbol{d}}_f$ is the relative velocity of the fluid with respect to the moving coordinate velocity.

The turbulence model employed in this study is *k*-*kl*-*ω* transition model (Walter and Cokljat 2008), which is an eddy-viscosity turbulence model based on the k-ω framework and includes laminar kinetic energy to represent the pre-transitional fluctuations in boundary layers. The pressure and velocity coupling is solved by the coupled algorithm with the second order scheme of pressure. The third-order MUSL scheme is adopted for the discretization of all the variables other than pressure. The *k*-*kl*-*ω* model was validated in similar attic settings by Wang et al. (2012)

The 3D model consists of about 200,000 to 600,000 hex elements owing to the geometry size difference in each model. A refined boundary layer consists of four layer elements is added at the bottom side of roof. All the calculations start from initial conditions of zero velocity and uniform temperature. The time step size is 1s with 20 iterations in each step. Numerical experiments show that decreasing the time step to 0.5 s or requiring 40 iterations in each time step generate negligible difference in solutions. The simulation converges with energy residual less than 10e-6 after about 3500 time steps.

Roof temperature collection

The roof and ambient temperatures employed in the case study refer to the temperature data recorded by Mississippi Forest Products Laboratory in Starkville, Mississippi, in 1999 (Winandy, Barnes, and Hatfield, 2000). According to Building

America climate zone divisions, Starkville is located in the Mixed-Humid zone and has relatively moderate weather conditions in winter and hot weather conditions in summer.

To reduce the computational cost, only one typical day for each season is selected from the temperature observation period. According to the climate statistics, the coldest and hottest days of the year usually appear in January and July in this region. Data in this two months was used to represent the winter and summer seasons in this study. Meanwhile, April and October, which have more mild temperatures, represent the spring and fall. The variances of temperature data in each hour of the four months are calculated and summarized. The smallest daily total variances are identified for each month. The days which had the closest daily temperatures to their monthly average were January 7th, April 28th, July 10th, and October 29th respectively in 1999. Thus these four days are selected to be a representative day of the corresponding season. And the temperature profile of roof and ambient temperature in the days was employed as the boundary conditions in the 3D CFD model.

In order to find the time series approximate functions of the 24-hour temperature profiles, the recorded roof and ambient temperature data in the four selected days are fitted into a four series Gaussian function respectively as listed in (7) using nonlinear least square fit method in Matlab. The R-squares are all above 0.99 which indicate a good match between the recorded data and the fitted data. The fitted functions then were applied to the 3D model as the boundary conditions.

$$f\left(x\right)=a_1e^{\left[\frac{(x-b_1)}{c_1}\right]^2}+a_2e^{\left[\frac{(x-b_2)}{c_2}\right]^2}+a_3e^{\left[\frac{(x-b_3)}{c_3}\right]^2}+a_4e^{\left[\frac{(x-b_4)}{c_4}\right]^2} \quad (7)$$

where x is time (s) and starts from 14400 s for each condition, to allow four hours before the start of each day are taken into account in the function fitting so as to improve the accuracy of the results; f(x) is in terms of "K"; a1, a2, a3, b1, b2, b3, c1, c2, c3 are constants, where a,b, and c represent amplitude, centroid and peak width respectively of the temperature curves. The results of the fitting are in Table 1.

Table 1. Value of constants in the fitted temperature functions

	7-Jan		**28-Apr**		**10-Jul**		**29-Oct**	
	Roof	**Ambient**	**Roof**	**Ambient**	**Roof**	**Ambient**	**Roof**	**Ambient**
$\mathbf{a_1}$	13.51	252	10.87	301.4	51.63	196.8	22.69	289.8
$\mathbf{a_2}$	285.9	217	11140	132.3	314.9	261.2	291.5	237
$\mathbf{a_3}$	35.8	98.37	13.7	49.89	-34.07	228	35.13	14.13
$\mathbf{a_4}$	4.43	230.1	39.41	9.165	271.4	53.88	42.58	132.6
$\mathbf{b_1}$	61780	55930	51610	63310	59380	99630	51560	64130
$\mathbf{b_2}$	91740	-13690	-12610000	-13270	115100	-9025	-40010	-14710
$\mathbf{b_3}$	-16730	18630	94350	111300	102400	53250	105600	22340
$\mathbf{b_4}$	26920	116900	61620	24230	-8697	109000	64120	115500
$\mathbf{c_1}$	10750	44380	4127	90510	18140	35930	8581	56780
$\mathbf{c_2}$	250200	27790	6614000	31750	73740	44910	371500	40910
$\mathbf{c_3}$	35550	25010	24550	21120	23980	42200	33230	15760
$\mathbf{c_4}$	20280	39890	14190	14000	72400	13210	13000	26740

Data processing

The mass flow rates in the recessed lighting and the heat transfer rates in the ceiling are calculated in CFD based on equation (5, 6) and exported from the simulation results. Then by using equations (8, 9), the energy loss rate of RLFs can be estimated.

$$m = V_m \Delta t \quad (8)$$

$$q_r = \frac{cm\Delta T}{\Delta t} = cV_m \Delta T_1 \quad (9)$$

where c is the specific heat capacity constant (J/kg•K) which equals to 1006 for the air; m is mass (kg); and ΔT_1 is the indoor and outdoor air temperature difference (K); Indoor air temperature equals to 293 K in winter, 297 K in summer, and 295 K in spring and fall; Δt is the duration of the energy loss(s);) V_m is the mass flow rate of air (kg/s); q_r is the heat transfer rate of the RLFs(W);

The conduction heat transfer rate of ceiling can be calculated by the following equation:

$$\mathrm{q}_c = h_c A \Delta T_2 \quad (10)$$

where q_c is the heat transfer rate of ceiling (W); A is the heat transfer area of the surface (m^2); h_c is convective heat transfer coefficient of the process which equals to 0.284 (W/m^2K); ΔT_2 is temperature difference between the surface and the bulk fluid (K).

The energy loss from the RLFs and the ceiling can be estimated by the following equation:

$$Q_r = \frac{q_r \times \Delta t}{1055 J/BTU} \quad (11)$$

$$Q_c = \frac{q_c \times \Delta t}{1055 J/BTU} \quad (12)$$

Where Q_r is the energy loss from the RLFs (BTU); Q_c is the energy loss from the ceiling (BTU)

While the percentage of energy loss from RLFs can be calculated by

$$RLFs\,\% = \frac{Q_r}{Q_c+Q_r} \quad (13)$$

Results and discussion

Winter condition

The 24 hour attic energy loss shows different characteristics in each season. As listed in equation (10), the energy loss rate of ceiling in this case study is determined by the temperature gradient at two sides of ceiling multiplied by two constant values for this case study. The temperature of the lower side of the ceiling is a constant value (293K), while the temperature of the upper side of the ceiling is determined by both radiation and air convection. In the nighttime, as shown in Fig. 4-A, the roof temperature has very small discrepancy with the outdoor temperature which results in a very low radiation effect. Thus, the temperature of upper side of the ceiling is mainly dominated by air convection. Since the difference between the outdoor and indoor air temperature is bigger in the nighttime, the energy loss from the ceiling exhibits a relatively high value (Fig. 4-C). In the daytime, as the roof temperature becomes higher than the outdoor temperature (Fig. 4-A), the radiation from the roof gradually increases. In the meantime, the difference between the indoor air and outdoor air temperature decreases. As a result, the energy loss from the ceiling decreases to a relatively low value in the daytime.

However, as shown in Fig. 4-C, the energy loss rate of recessed lighting has an adverse effect. As listed in equation (9), the energy loss from the recess lighting is determined by the mass flow rate of the air leakage which is calculated by equation (5, 6), as well as the indoor and outdoor air temperature difference. Although the temperature difference is smaller in the daytime, the energy loss rate of recess lighting is larger than that in the nighttime. This is due to the fact that the rise of the roof temperature intensifies the soffit-ridge ventilation which results in the increase of the mass flow rate of the leakage air in the recess lighting, as shown in Fig. 4-B. The streamlines and contour of temperature of the recessed lighting are shown in Fig. 5.

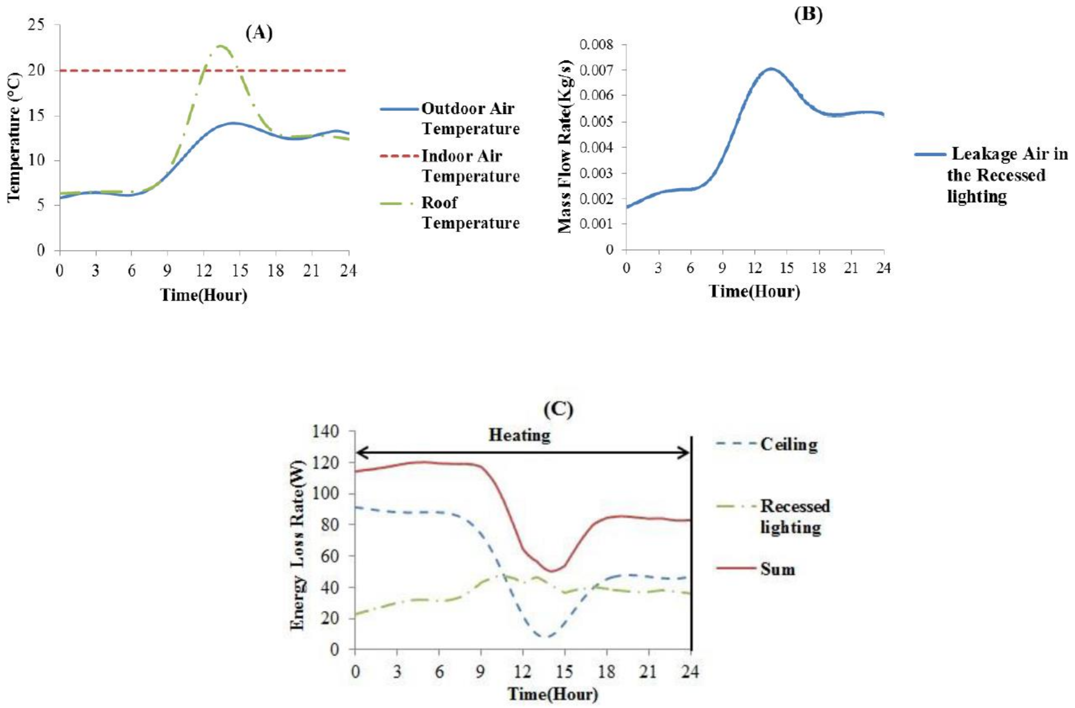

Fig. 4. Temperature data (A), mass flow rate of the leakage air in recessed lighting (B), and 24 hour attic energy loss (C) on 1/7/1999

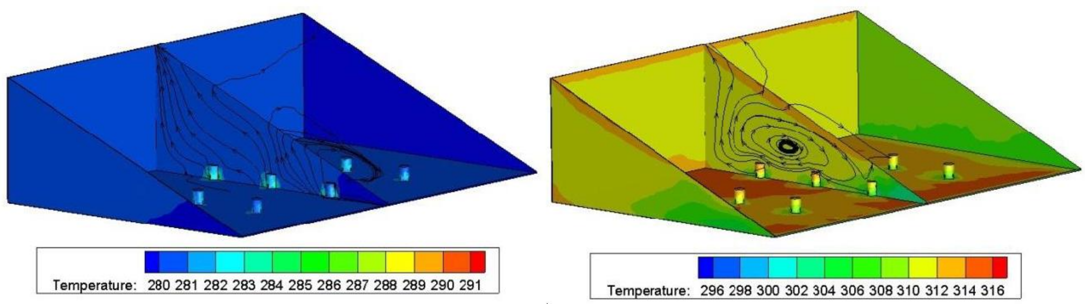

Fig. 5. Streamlines and contour of temperature in the nighttime (left) and in the daytime (right) on 1/7/1999

Spring condition

In spring, the energy consumption for maintaining the indoor air temperature is from both the heating load and the cooling load (Fig. 6-C). Other than the mass flow rate in January, which is positive anytime, the mass flow rate in April appears negative in the nighttime, as shown in Fig. 6-B. This means that rather than in January when the indoor air enters through the bottom of the canister, rises up and goes out from the ridge vent (Fig. 5), the air flow is in an opposite directions during the nighttime in spring (Fig. 6-A). The primary cause of the phenomena is that the roof temperature becomes lower than the outdoor temperature. Compared with the heating effect of the celling, the cooling effect of the roof is more intense. As a cold source, the roof reduces the outdoor ambient air temperature, and increases the density of the air, which makes the outdoor air flow into the attic and then leaks into the home from recessed lightings. However, the outdoor air and roof temperature difference is relatively small, thus the energy loss amount from the recessed lighting is small during this time compared to winter time.

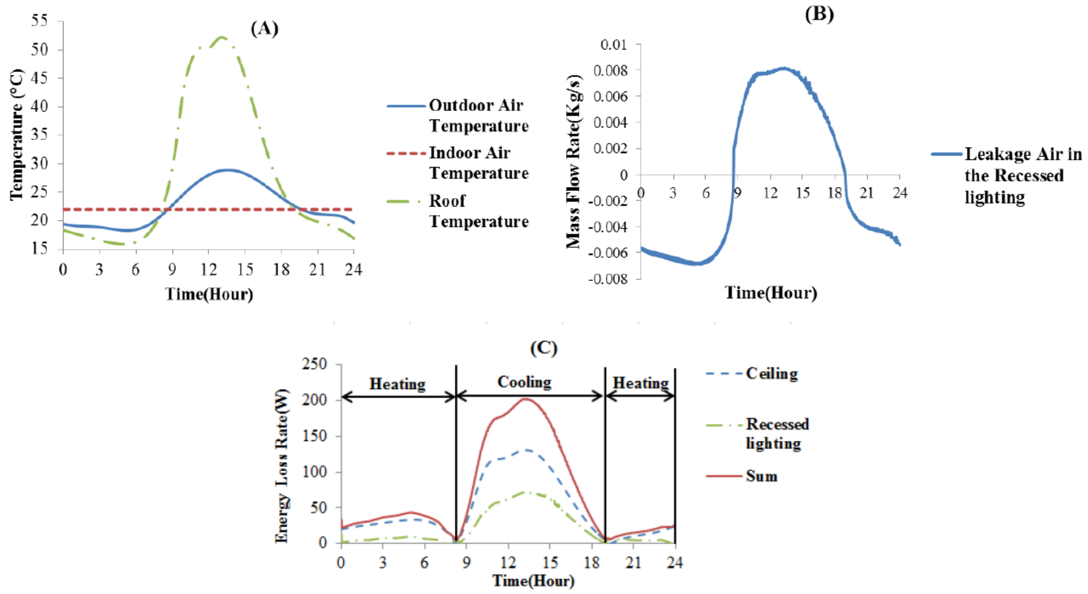

Fig. 6. Temperature data (A), mass flow rate of the leakage air in recessed lighting (B), and 24 hour attic energy loss (C) on 4/28/1999

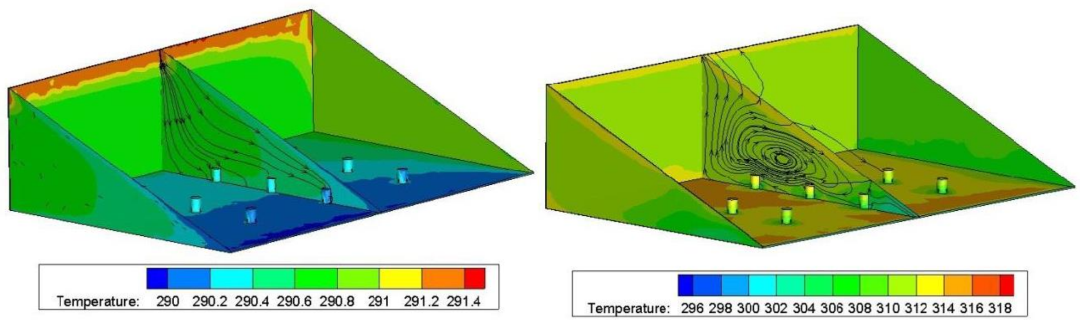

Fig. 7. Streamlines and contour of temperature in the nighttime (left) and in the daytime (right) on 4/28/1999

In the daytime, as the roof temperature rises higher than the outdoor temperature, the roof becomes a heating source which increases the temperature of the air in the attic and decreases the air density. This makes the indoor air rise, and leak into the attic and form a convection cell, as shown in Fig. 7 (Right). In addition, other than in January, the energy loss from the ceiling becomes more significant in the daytime in April (Fig. 6-C), which is due to the bigger indoor and outdoor temperature difference (Fig. 6-A).

Summer condition

Due to the warm climate in the Mixed-Humid zone, the feature of the energy loss in summer is generally similar to that in spring. However, the energy loss rate for both ceiling and recessed lighting becomes bigger. In addition, the duration of the heating time is shorter. Even though the indoor air temperature set in the case study is only a little higher than the outdoor air temperature from 12 a.m. to 6 a.m. as shown in Fig. 8-A, this temperature difference can result in the emergence of the heating load (Fig. 8-C). As the outdoor air and roof temperatures gradually fall down after 1 p.m., the cooling load also begins to reduce. When close to 12 p.m., as the outdoor and roof temperature approach the indoor temperature, the energy loss rate of both ceiling and recessed lighting, becomes close to zero. Thus, the heating load appears when the outdoor air and roof temperatures are lower than the indoor temperature even though it is in summer.

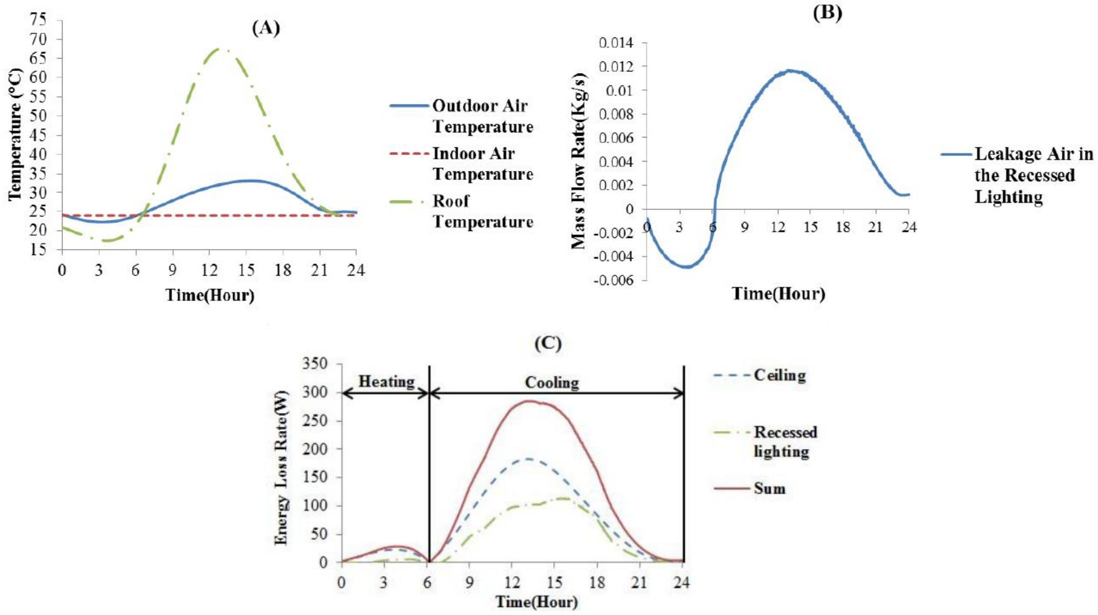

Fig. 8. Temperature data (A), mass flow rate of the leakage air in recessed lighting (B), and 24 hour attic energy loss (C) on 7/10/1999

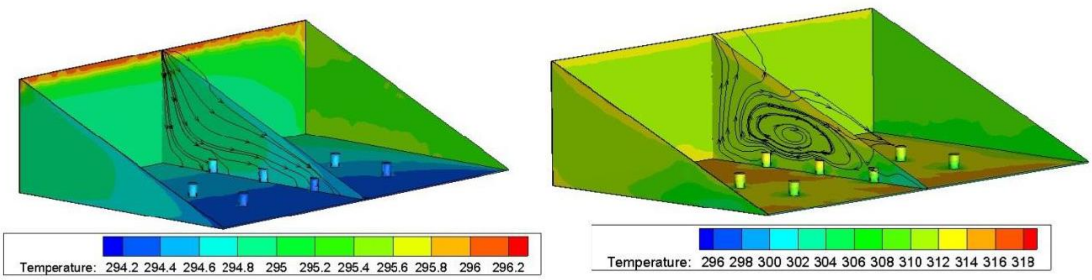

Fig. 9. Streamlines and contour of temperature in the nighttime (left) and in the daytime (right) on 7/10/1999

Fall condition

As shown in Fig. 10-C, the curve of the energy loss rate of the recessed lighting shows more fluctuations than that in the other seasons. This is due to the fact that the outdoor air and the roof temperatures reach the value of the indoor air temperature at different times respectively. As the mass flow rate of the leakage air in the recess lighting approaches zero, the energy loss from the recessed lighting tends to be zero at the first time. In addition, when the other energy loss determinant, the indoor and outdoor air temperature difference, as listed in Equation (6), reaches zero around 10:30 a.m., the energy loss from the recessed lighting falls to zero at the second time.

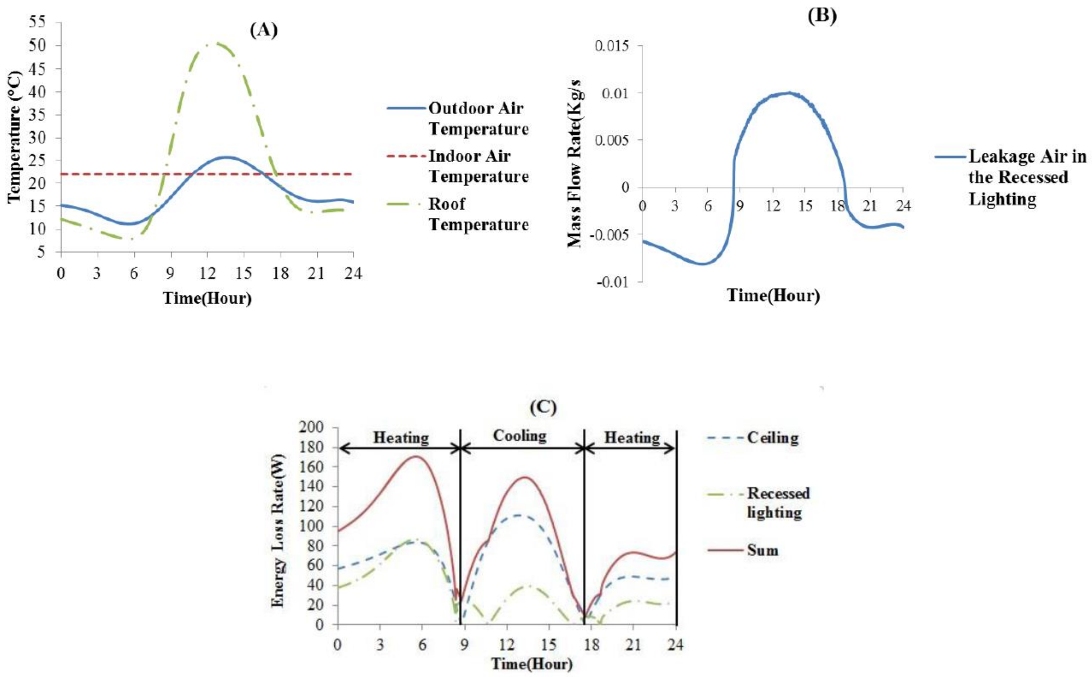

Fig. 10. Temperature data (A), Mass Flow Rate of the Leakage Air in Recessed Lighting (B), and 24 Hour Attic Energy Loss (C) on 10/29/1999

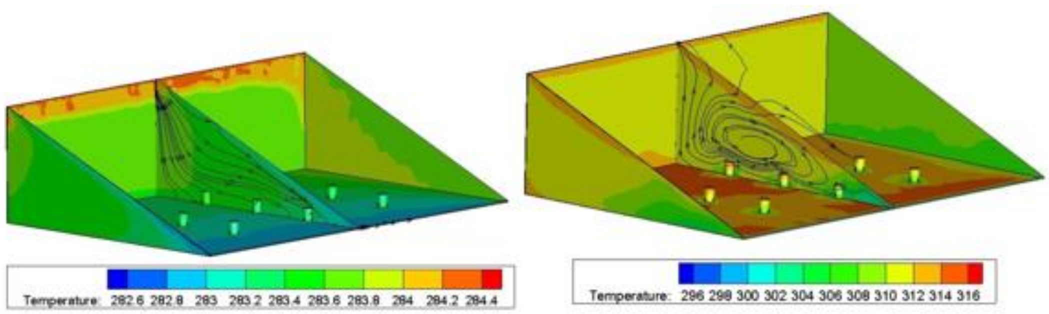

Fig. 11. Streamlines and contour of temperature in the nighttime (left) and in the Daytime (right) on 10/29/1999

The 24 hour energy losses from the nine RLFs and the ceiling in each season that are calculated by equation (11, 12), and the percentages of energy loss from the RLFs which are calculated by equation (13) are summarized in Table 3. As shown in the table, the energy losses caused by the RLFs in the four seasons are all significant. In winter and summer, under the impacts of the energy loss from the recessed lighting and ceiling, the heating load and cooling load reach their highest points respectively (Fig. 4-C, Fig. 8-C). Even though in spring and fall when the climate in the Mixed-Humid zone is relatively moderate, the energy loss from the recessed lighting is still considerable. As shown in Fig. 12, the percentages of the energy loss from recessed lighting are all above thirty percent all over the year and as high as eighty percent in winter, which numerically verifies the energy impact of the air leakage problem in the recessed lighting.

Table 2. Hourly Energy Loss from the RLFs, Total Energy Loss through the Attic, and RLF Loss Percentage

	Hourly Energy Loss (BTU)											
	1/7/1999			4/28/1999			7/10/1999			10/29/1999		
	RLF	**Attic**	**RLF%**	**RLF**	**Attic**	**RLF%**	**RLF**	**Attic**	**RLF%**	**RLF**	**Attic**	**RLF%**
0	82.3	391.7	21.0%	50.9	126.0	40.4%	2.4	21.6	11.3%	136.2	338.2	40.3%
1	90.5	395.7	22.9%	58.3	143.7	40.6%	1.3	46.5	2.8%	159.6	376.8	42.3%
2	98.9	400.7	24.7%	65.3	159.4	40.9%	9.1	76.0	11.9%	195.5	430.7	45.4%
3	106.	406.1	26.1%	71.5	174.7	40.9%	17.5	95.4	18.4%	236.9	492.7	48.1%
4	109.	409.1	26.7%	77.1	188.2	41.0%	20.8	92.0	22.6%	265.0	540.4	49.0%
5	108.	408.6	26.5%	75.1	187.8	40.0%	13.8	52.6	26.3%	279.5	565.0	49.5%
6	108.	406.6	26.6%	64.1	162.5	39.5%	1.9	33.4	5.8%	270.1	540.2	50.0%
7	116.	406.0	28.6%	38.4	96.3	39.9%	31.6	157.1	20.1%	193.7	394.9	49.1%
8	134.	403.5	33.4%	6.2	46.8	13.2%	111.	349.4	31.9%	75.3	132.4	56.9%
9	153.	382.9	40.2%	42.1	248.6	16.9%	182.	541.1	33.7%	59.3	188.5	31.5%
10	160.	331.5	48.5%	113.	482.7	23.5%	245.	717.8	34.2%	15.6	286.5	5.4%
11	153.	258.1	59.4%	149.	555.4	26.9%	311.	873.3	35.6%	58.3	407.2	14.3%
12	153.	204.5	74.9%	174.	605.1	28.8%	341.	953.8	35.8%	101.8	478.1	21.3%
13	150.	179.8	83.5%	186.	627.3	29.7%	349.	968.0	36.1%	116.7	489.2	23.9%
14	132.	176.3	75.2%	173.	571.1	30.4%	369.	951.3	38.9%	110.3	440.6	25.0%
15	129.	209.0	61.7%	135.	447.6	30.3%	385.	897.8	42.9%	82.8	325.5	25.4%
16	135.	253.9	53.3%	83.6	294.0	28.4%	355.	780.7	45.5%	23.7	148.6	16.0%
17	135.	281.5	48.2%	39.3	154.8	25.4%	294.	626.9	47.0%	28.5	56.5	50.5%
18	131.	290.4	45.1%	8.5	50.7	16.8%	195.	436.8	44.8%	23.2	115.0	20.2%
19	128.	290.9	44.0%	3.0	12.3	24.3%	101.	259.9	39.1%	53.4	202.0	26.5%
20	126.	288.1	44.0%	7.5	35.9	20.8%	50.1	140.6	35.7%	72.6	238.8	30.4%
21	128.	286.8	44.9%	12.7	53.8	23.6%	22.9	65.5	35.0%	77.0	242.1	31.8%
22	128.	284.4	45.2%	13.9	67.5	20.6%	8.9	26.1	34.1%	74.0	233.6	31.7%
23	125.	282.7	44.2%	27.7	101.5	27.3%	4.5	15.3	29.4%	75.8	237.0	32.0%
	3026	7628.7	39.7%	1677	5593.9	30.0%	3427	9179.0	37.3%	2784.	7900.4	35.2%

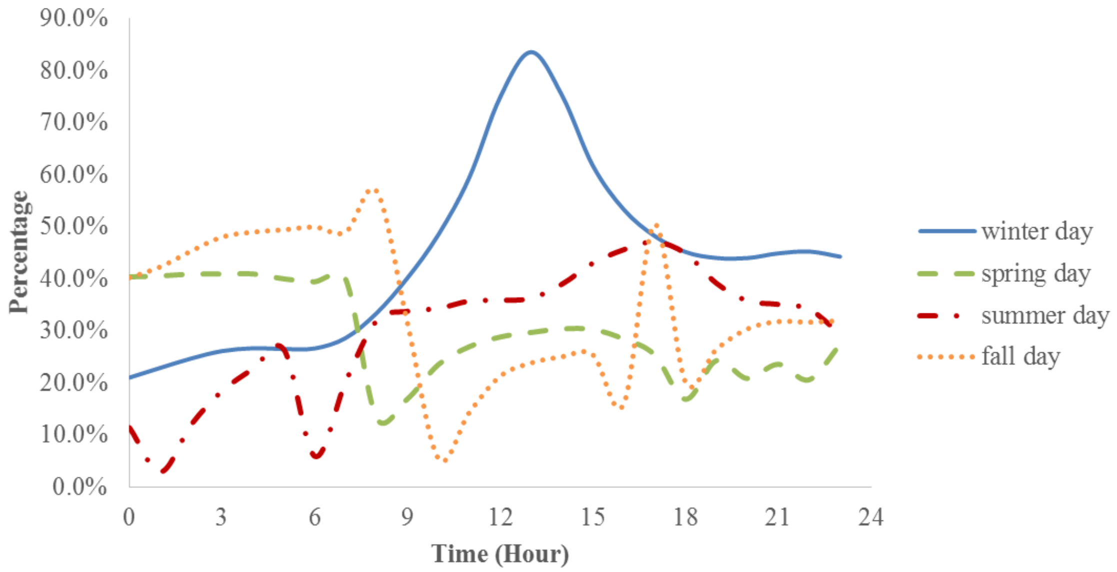

Fig. 12. Percentage of the energy loss from recessed lighting

Estimate of the energy loss from recessed lighting in the mixed-humid zone

Considering different climate regions and different roof/attic configurations we understand that the energy loss per household presented in this study is just a rough estimate in terms of magnitude. Twenty to forty RLFs per household are used in the estimate, according to the related literature (Van der Meer, 2002). The two cases are considered in the estimation: in first case, all the twenty to forty RLFs are assumed on the attic ceiling, while in the second case only half of the RLFs (10~20) are assumed on the attic. No matter which case, as shown in Table 4, the annually energy loss from RLFs is considerable. Considering that the number of the homes that have unfinished attics without air conditioning in the Mixed-Humid climate zone is 10.2 million (U.S EIA 2009), the monthly energy loss from the recessed lighting in the whole region is quite substantial.

Table 4. The Energy Loss from Recessed Lighting per Household in the Case Study

	24 Hour Energy Loss			Monthly Energy Loss		Seasonal Energy Loss	
	Per RLF (BTU)	Per Household in the Mixed-humid Zone (MBTU)					
		10-20 RLFs	20-40 RLFs	10-20 RLFs	20-40 RLFs	10-20 RLFs	20-40 RLFs
Jan	336	3.3-6.7	6.7~1.3	104.2~208.5	208.5~416.9	416.9~ 833.8	833.8~ 1,667.7
Apr	186	1.9-3.7	3.7~7.4	55.9~111.9	111.9~223.7	223.7~ 447.4	447.4~ 894.8
Jul	381	3.8-7.6	7.6~15.2	118.1~236.1	236.1~472.3	472.2~ 944.5	944.5~ 1,889.1
Oct	309	3.1-6.1	6.2~12.3	95.9~191.8	191.8~383.7	383.6~ 767.3	767.3~ 1,534.7
Annual Sum						1,496.6~ 2,993.2	2,993.2~ 5,986.5

Conclusions

In this paper the authors presented a quantitatively investigation of the energy loss due to the air leakage through the RLFs. Even though the climate is relatively moderate in the Mixed-Humid zone, the results of the simulations indicate RLFs can still be a very significant source of energy loss all over the year, which indicates that in residential buildings significant amount of energy is wasted due to the leakage through RLFs.

Though there are a lot of limitations in this study (such as not considering light-on case, moisture and vapor, wind effects, non-vented attics and etc.), which makes it only a rough estimate, the results of the case study still provide some evidence for the significant energy waste due to the air leakage through RLFs. The study suggests that systematic approach is needed to improve the RLF design and construction practice to reduce or remove the RLF's negative impact on energy loss of residential buildings.

Acknowledgement

The authors of this paper would like to express our sincere appreciation to Dr. Jerrold Winandy for providing us with the multi-year temperature data collected by USDA Forest Products Lab. Dr. Winandy retired from Project Leader position of the Engineered Composites Science Research Work Unit at the lab in 2008.

Notation

The following symbols are used in this paper:

A = the heat transfer area of the surface (m^2);

$\mathrm{a}_1, \mathrm{a}_2, \mathrm{a}_3, \mathrm{b}_1, \mathrm{b}_2, \mathrm{b}_3, \mathrm{c}_1, \mathrm{c}_2, \mathrm{c}_3$ = constants;

c = the specific heat capacity constant $(\mathrm{J/kg \cdot K})$;

$\dot{\boldsymbol{d}}_\mathrm{f}$ = Moving coordinate velocity;

F_{ij} = the view factor;

$\mathrm{f}(\mathrm{x})$ = the roof or outdoor ambient air temperatures (K);

$\boldsymbol{f}_\mathrm{f}^\mathrm{B}$ = Body forces perunit volume;

h_c = convective heat transfer coefficient of the process $(\mathrm{W/m^2K})$;

i = finite surface;

j = finite surface;

k = finite surface;

m = mass (kg);

Q = the energy loss from the RLFs (J);

$\mathrm{q}_{\mathrm{out,k}}$ = the energy flux leaving the surface k (W);

$\mathrm{q}_{\mathrm{out,j}}$ = the energy flux leaving the surface j (W);

$\mathrm{q}_{\mathrm{in,k}}$ = the energy flux incident on the surface from the surroundings (W);

q_r = the heat transfer rate of the RLFs (W);

q_c = the heat transfer rate of ceiling (W);

T_k = the temperature at the surface k (K)

$\Delta\mathrm{T}_1$ = the indoor and outdoor air temperature difference (K);

$\Delta\mathrm{T}_2$ = temperature difference between the surface and the bulk fluid (K);

$\Delta\mathrm{t}$ = the duration of the energy loss (s);

V_m = the mass flow rate of air $(\mathrm{kg/s})$;

$\mathbf{v}$ = Fluid velocity vector;

x = time (s)

δ_{ij} = Kronecker delta

ε_k = Emissivity

ρ_f = Fluid density

σ = Boltzmann constant

$\boldsymbol{\tau}_\mathrm{f}$ = Fluid stress tensor

References

Armando, L and. McCarthy, S. (2000). A Recessed Can of Worms. *Home Energy.* < http://www.waptac.org/data/files/Website_docs/Training/Standardized_Curricula/Curricula_Resources/Armanda_A-Recessed-Can-of-Worms.pdf > (March. 1 2013)

Baker, J., and Lugano, F. (1999). A passive approach to practical climate control. *In Postprints of the Wooden Artifacts Group (American Institute for Conservation of Historic and Artistic Works. Wooden Artifacts Group),* 34–45. Washington, DC: American Institute for Conservation of Historic and Artistic Works, Wooden Artifacts Group.

Balaras, C. and A. Argiriou (2002). "Infrared thermography for building diagnostics." *Energy and buildings* 34(2): 171-183.

CEC (California Energy Commission) (2013). “California Title 24, Section 6.3.12”. Sacramento, CA

Emmerich, S. J., McDowell, T. P., and Anis, W. (2005). Investigation of the impact of commercial building envelope airtightness on HVAC energy use. US Department of Commerce, Technology Administration, National Institute of Standards and Technology.

Home Depot (2015). “Recessed Lighting Applications” <http://www.homedepot.com/hdus/en_US/DTCCOM/HomePage/Know_How/Brand_Pages/Lighting_Fans/Halo/Docs/RecessedPlanningPad.pdf >(Sep. 30, 2015)

ICC (International code council) (2012) “International Energy Conservation Code, Section 402.4”, Country Club Hills, IL.

Jokisalo, J., Kalamees, T., Kurnitski, J., Eskola, L., Jokiranta, K., & Vinha, J. (2008). A comparison of measured and simulated air pressure conditions of a detached house in a cold climate. *Journal of Building Physics*, 32(1), 67-89.

Persily, A. (2004) "QandA on building security." *ASHRAE Journal* 46(9):20-23.

Plympton, P. C., Dagher, L., and Zwack, W. (2007). *Industry Stakeholder Recommendations for DOE's RD&D for Increasing Energy Efficiency in Existing Homes*. National Renewable Energy Laboratory.

Savers, E. (2006). *Tips on saving money and energy at home.* Washington DC: US Department of Energy, Oct, 12, 2006.

SBCC (Washington State Building Code Council). (2009). "Washington State Building Code, Section 502.4.4" Olympia, WA.

Sherman, M. H. and D. J. Dickerhoff (1998). "Airtightness of US dwellings." *Transactions-American Society Of Heating Refrigerating And Air Conditioning Engineers* 104: 1359-1367.

U.S Energy Information administration, (2009). Structural and Geographic Characteristics of U.S. Homes, by Climate Region, <http://www.eia.gov/consumption/residential/data/2009/#structural> (Mar. 1, 2013)

Van der Meer, B. (2002). Air leakage in recessed lighting *Builder Brief*: The Pennsylvania Housing Research/Resource Center.

Wang, S., and Shen, Z. [a] (2012). Impacts of ventilation ratio and vent balance on cooling load and air flow of naturally ventilated attics. *Energies* 5(9), 3218-3232.

Wang, S. and Shen, Z. [b] (2012). "Effects of roof pitch on air flow and heating load of sealed and vented attics for gable-roof residential buildings." *Sustainability* 4(9): 1999-2021.

Wang, S., Shen, Z., and Gu, L. (2012). "Numerical simulation of buoyancy-driven turbulent ventilation in attic space under winter conditions." *Energy and buildings* 47: 360-368.

Wanyu R. Chan, Phillip N. Price, Michael D. Sohn, Ashok J. Gadgil. (2003). Analysis of U.S Residential air leakage database: Lawrence Berkeley National Laboratory.

Winandy, J. E., Barnes, H. M., & Hatfield, C. A. (2000). *Roof temperature histories in matched attics in Mississippi and Wisconsin*. US Department of Agriculture, Forest Service, Forest Products Laboratory.

Walters, D. K., and Cokljat, D. (2008). A three-equation eddy-viscosity model for Reynolds-averaged Navier–Stokes simulations of transitional flow. Journal of Fluids Engineering, 130(12), 121401.

Younes, C., Shdid, C. A., and Bitsuamlak, G. (2012). Air infiltration through building envelopes: A review. *Journal of Building Physics*, 35(3), 267-302. doi: Doi 10.1177/1744259111423085